(Received 2 October 2024, Accepted 8 January 2025, Scheduled 19 January 2025)

Design and Performance Evaluation of a High-Isolation MIMO Antenna Array for 5G N77/N78/N79 and WLAN Implementations

Juhui Zhang[1], Wei Luo[2], Qiangjuan Li[1], Yuexiao Pan[1,*], and Gui Liu[2,*]

[1] *College of Chemistry & Materials Engineering, Wenzhou University, Wenzhou 325035, Zhejiang, China*
[2] *College of Electrical and Electronics Engineering, Wenzhou University, Wenzhou 325035, Zhejiang, China*

ABSTRACT: This paper proposes a broadband multi-input multi-output (MIMO) antenna array operating in the 3.3–6 GHz frequency range. The antenna array consists of eight identical Z-shaped radiation elements, and the coupling between the antenna elements is minimized through the use of an optimized defected ground structure. Each antenna element is composed of a modified Z-shaped radiation strip, an opposing L-shaped strip, and a rectangular strip. Based on simulation and measurement results, it can be concluded that the antenna array meets the -10 dB bandwidth requirement within the desired frequency band, with the transmission coefficient of less than -15 dB and an envelope correlation coefficient (ECC) below 0.006. Additionally, the proposed antenna achieves a maximum gain ranging from 2.6 to 8 dBi, with an efficiency exceeding 76%. The overall size of the phone antenna is $150 \times 75 \times 7$ mm^3, while each antenna element measured only 7.8 mm $\times$ 7 mm $\times$ 0.8 mm ($0.091\lambda \times 0.082\lambda \times 0.009\lambda$, where λ represents the wavelength at 3.5 GHz). The high-isolation broadband MIMO antenna proposed in this study emerges as a promising candidate for fifth-generation (5G) New Radio (NR) and WLAN applications.

1. INTRODUCTION

In recent years, the explosive growth of communication data has pushed fourth-generation (4G) mobile communication systems to their limits [1]. Researchers have turned their attention to fifth generation (5G) wireless communication technologies [2–4]. 5G mobile communication has now entered the commercial stage, promising high throughput, low latency, and reduced energy consumption [5, 6]. As the next frontier in compact communication technology, 5G mobile networks represent the latest key solution for wireless technology bands [7]. Operating within the 5G NR spectrum below the sub-6 GHz band, including n77 band (3300–4200 MHz), n78 band (3300–3800 MHz), and n79 band (4400–5000 MHz), these networks may not fully satisfy the requirements of multi-band communication for 5G mobile phones. Additionally, the unique WLAN spectrum (5150–5925 MHz) has also garnered significant interest [8].

The introduction of fifth generation mobile communication (5G) brings with it the promise of higher data transmission rates. To meet this demand, multiple input multiple output (MIMO) technologies must be integrated into 5G wireless communication systems, as large-scale MIMO systems can provide increased channel capacity [9–11]. As the core technology of 5G communication system, MIMO provides increased channel capacity, alleviates multipath fading, and provides faster communication, significantly improves spectral efficiency without increasing power and spectrum usage, and is widely used in the design of terminal antennas to enhance 5G communication capabilities [12, 13].

Building a MIMO antenna for terminal design requires a minimum of 6–8 elements. However, due to the limited size of smartphones, the coupling effect between antenna elements can be quite pronounced, making decoupling a challenging task [14–16]. Tight coupling between antenna elements can lead to low isolation, low antenna efficiency, and high peak SAR values. Integrating multiple antennas into smartphones presents its own set of challenges. As a result, existing technologies are being employed to reduce the coupling between closely spaced antenna elements [17]. Four or eight antenna elements can be arranged in different regions, allowing for enhanced isolation by directly adjusting the spatial distance between them. Other methods exist to reduce mutual coupling between closely located antenna elements. The first method involves adding a new coupling path between antenna elements to counteract the original coupling, often in the form of a neutral line or a decoupling element [18–20]. The second method entails blocking the coupling path using a defected ground structure or ground crack [21, 22]. The third method employs the decoupling method of the matching network. Although this method has the disadvantage of narrow bandwidth, it can reduce high coupling between antenna elements through orthogonal polarization [23], high-order mode [24], and other techniques. Realizing broadband decoupling of antenna arrays will be a new challenge and a future development trend for 5G smartphone antennas [25, 26].

* Corresponding authors: Yuexiao Pan (yxpan@wzu.edu.cn); Gui Liu (iitgliu2@gmail.com).

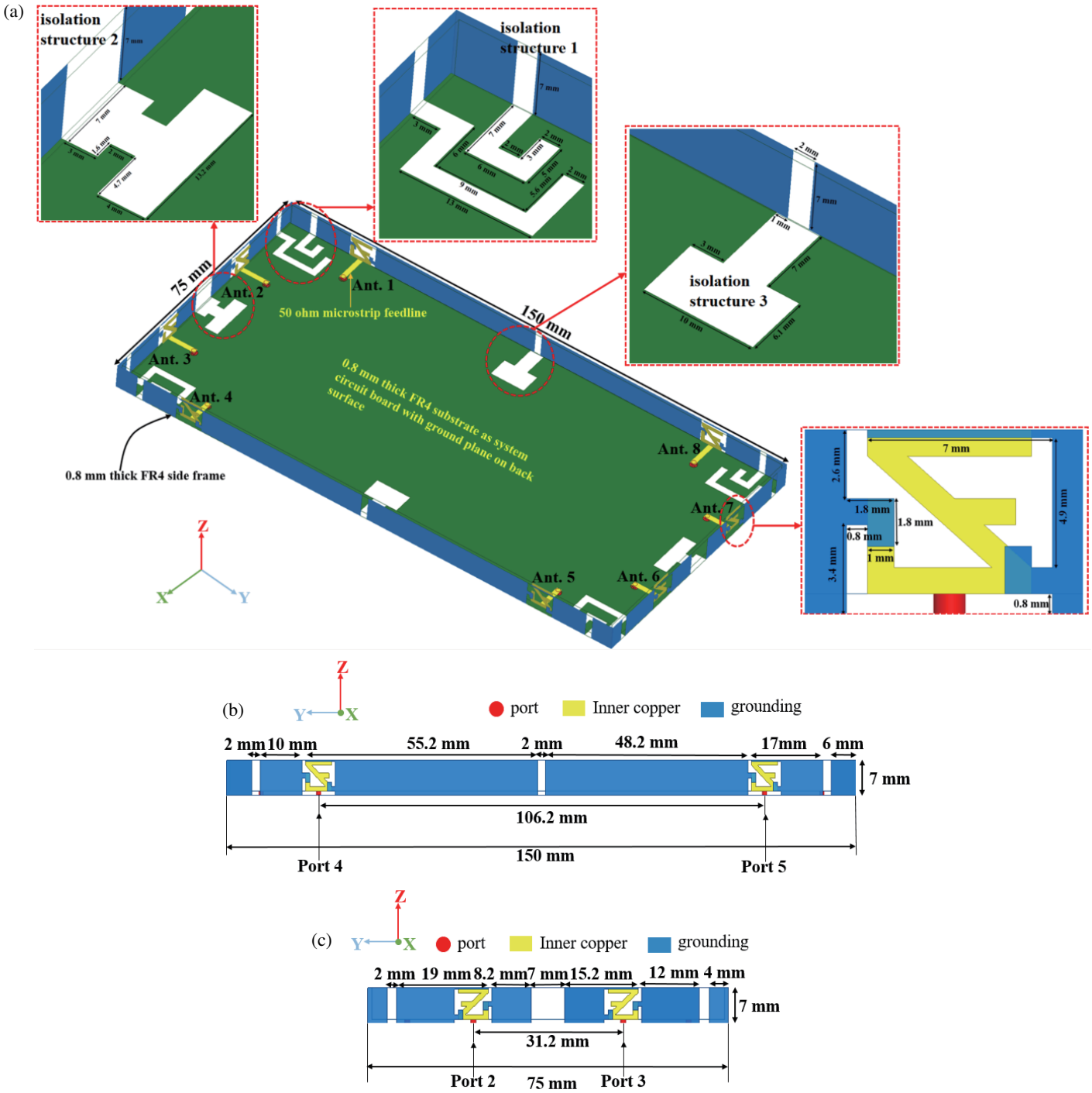

FIGURE 1. Geometry and dimensions of the proposed triple-band MIMO antenna array in millimeters. (a) Perspective view. (b) Front view. (c) Left view.

In this paper, we propose a broadband MIMO antenna array designed for the 5G NR n77 band (3300–4200 MHz), 5 GHz band (4400–5000 MHz), and WLAN frequencies (5150–5925 MHz). The −10 dB impedance bandwith of the proposed antenna is 2.7 GHz which operates in the frequency range of 3.3–6.0 GHz. The antenna array consists of eight identical elements and features an optimized defect ground structure to enhance isolation. Each antenna element is composed of a modified Z-shaped radiation strip, an opposing L-shaped strip, and a rectangular strip. The proposed compact broadband antenna achieves a small volume of just $7.8 \times 7 \times 0.8\,\text{mm}^3$. Within the frequency band of interest, the isolation is maintained at less than −15 dB, the ECC value below 0.006, and the efficiency can exceed 76%. The presence of the designed defected ground structure (DGS) effectively reduces interactions between the antenna elements.

2. ANTENNA GEOMETRY AND DESIGN

2.1. 8 Element MIMO Design

The geometry and dimensions of the triple-band MIMO antenna array are proposed and illustrated in Fig. 1. In this design, each antenna element has a precise size of $7.8 \times 7\,\text{mm}^2$ and is printed on an affordable FR-4 substrate ($\varepsilon r = 4.4$ and $\tan\delta = 0.02$), which is 0.8 mm thick. For the printed main circuit board (PCB), an FR-4 substrate measuring $150 \times 75 \times 0.8\,\text{mm}^3$ is chosen. The long sideboards measure $150\,\text{mm} \times 6.2\text{mm} \times 0.8\,\text{mm}$, and the short sideboards measure $75\,\text{mm} \times 6.2\,\text{mm} \times 0.8\,\text{mm}$. These sideboards, also made of FR-4 substrates, are vertically placed on the mainboard. Each antenna element is fed by a 50-Ω microstrip feedline with a width of 1.5 mm, connected to a 50 Ω SMA connector via a hole from the backside of the mainboard. Additionally, a $150 \times 75\,\text{mm}^2$ system ground plane is inscribed on the lower surface of the mainboard. L-shaped slots are etched in the corners of the ground plane to improve isolation. Each L-shaped slot is positioned between two antenna elements. To prevent coupling between the antenna elements on the long side, a T-shaped slot is etched in the middle. The arrangement of antenna elements and the separation between the antennas are shown in Figs. 1(a)–(c).

2.2. Single Antenna Element

Figure 2 shows a Z-shaped antenna feature, which is a triple-band antenna operating in the frequency bands of 3.3–4.2 GHz, 4.4–5.0 GHz for 5G communication, and 5.15–5.925 GHz for WLAN operation. The design parameters are as follows: $W_1 = 1$, $W_2 = 2.6$, $W_3 = 2.6$, $W_4 = 1.5$, $W_5 = 2.6$, $W_6 = 3.6$, $L_1 = 6.2$, $L_2 = 4.7$, $L_3 = 2.31$, $L_4 = 3.7$, $L_5 = 8$, $R_1 = 0.6$, all in millimetres. Additionally, this proposed antenna element has the advantage of a small volume, with each antenna element measuring only $7.8\,\text{mm} \times 7\,\text{mm}$.

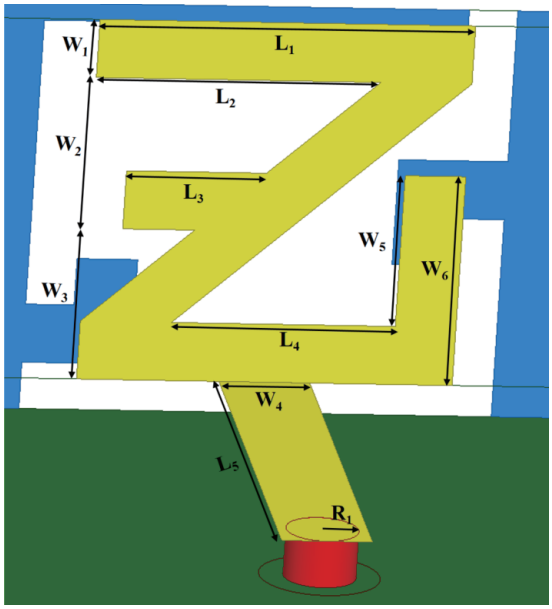

FIGURE 2. Detailed structure of the single antenna element.

3. DESIGN EVOLUTION PROCESS AND PARAMETRIC STUDY

In this section, we will demonstrate the evolutionary design process of the proposed triple-band MIMO antenna element. To better grasp the theory behind the proposed antenna element, a parametric study including design evolution, reflection coefficient, simulated surface current distribution, transmission coefficients, and optimal parameter analysis has been presented to further analyze the operational mechanism of the proposed triple-band antenna element.

The evolution and reflection coefficients of the triple-band antenna element are illustrated in Fig. 3. Case 1 is mainly a deformed Z-shaped antenna, and it can be seen that the reflection coefficient of the antenna is poor in this case. In order to reduce the return loss in the whole frequency band, a rectangular strip is introduced at the top of the rectangular slot in Case 2, which can greatly optimize the S-parameter, and an L-shaped rectangular strip with the opening facing upwards is added to the left of the rectangular slot in Case 3, which can optimize the resonant frequency of the high frequency to reduce the return loss of the high frequency, while the resonant frequency of the low frequency is maintained. In order to further reduce the return loss at the resonance point of the low frequency, Case 4 is designed. By adding an L-shaped rectangular strip with the opening facing down on the right side of the rectangular slot, the return loss of the low frequency can be greatly improved, so that the -10 dB impedance band of this antenna element reaches 3.26–6.09 GHz, which can well cover the 5G band of 3.3–4.2 GHz, 4.4–5.0 GHz, as well as 5.15–5.925 GHz of the WLAN band.

The simulation results depicting the antenna surface current distribution at 3.5 GHz, 4.7 GHz, and 5.5 GHz are presented in Fig. 4. At 3.5 GHz, the current distribution on the antenna surface is primarily concentrated on the rectangular strip at the top of the rectangular groove and the right side of the ring Z-shaped strip. At 4.7 GHz, the current distribution is mainly concentrated on the right part of the rectangular strip at the top of the rectangular groove and the middle part of the Z-shaped strip. Finally, at 5.5 GHz, the surface current distribution is predominantly focused on the middle part of the Z-shaped strip.

Figure 5 displays the simulated reflection coefficients of the proposed triple-band antenna with varying values of W_5 and L_1. When adjusting the height and length parameters while keeping other parameters fixed, the resonant frequencies can be effectively modified. For instance, when W_5 is set to 2.6 mm, the -10 dB impedance bandwidth spanning 3.26–6.09 GHz is achieved, effectively covering the desired frequency bands for 3.3–4.2 GHz, 4.4–5.0 GHz for 5G communication, and 5.15–5.925 GHz for WLAN. Similarly, by setting L_1 to 6.2 mm, the -10 dB impedance bandwidth adequately meets the requirements of the target frequency bands, as demonstrated in Fig. 5.

Figure 6 illustrates the simulated reflection coefficients and transmission coefficients of the proposed antenna array with and without an isolation structure. Due to the antenna's symmetric structure, only parameters including S_{11}, S_{22}, S_{33}, S_{44}, S_{12}, S_{13}, S_{14}, S_{18}, and S_{32} will be showcased. A comparison between the antennas with and without the isolation structure is presented in Fig. 6 to highlight the differences in reflection

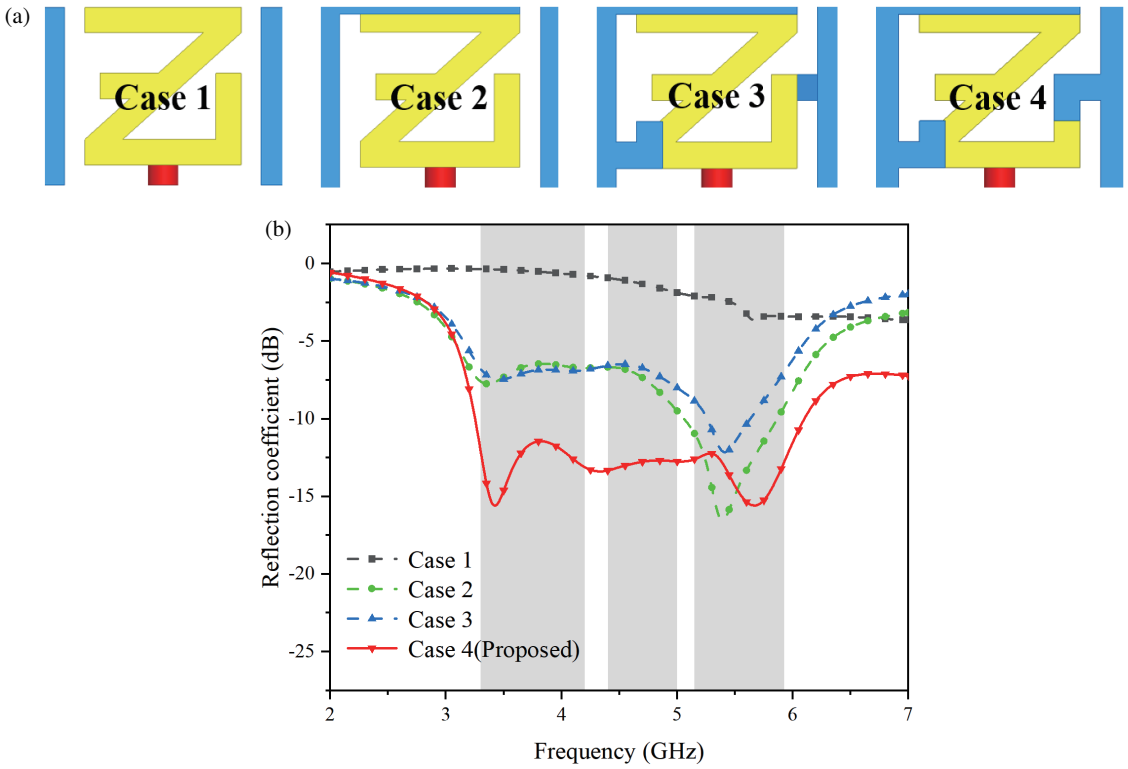

FIGURE 3. Design evolution of triple-band antenna element: (a) Design evolution. (b) Reflection coefficients.

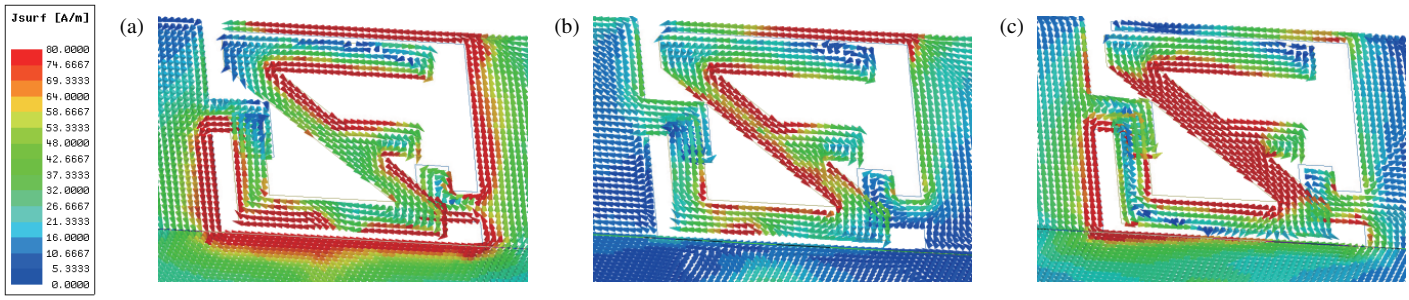

FIGURE 4. Simulated surface current distribution at (a) 3.5 GHz. (b) 4.7 GHz. (c) 5.5 GHz.

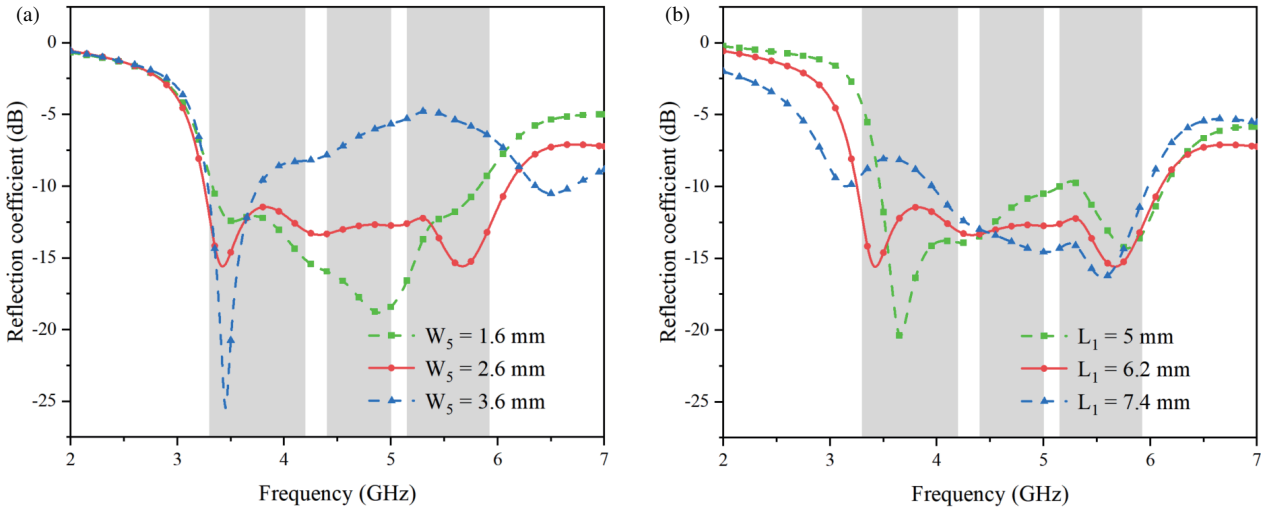

FIGURE 5. Simulated reflection coefficients with different values of (a) W_5. (b) L_1.

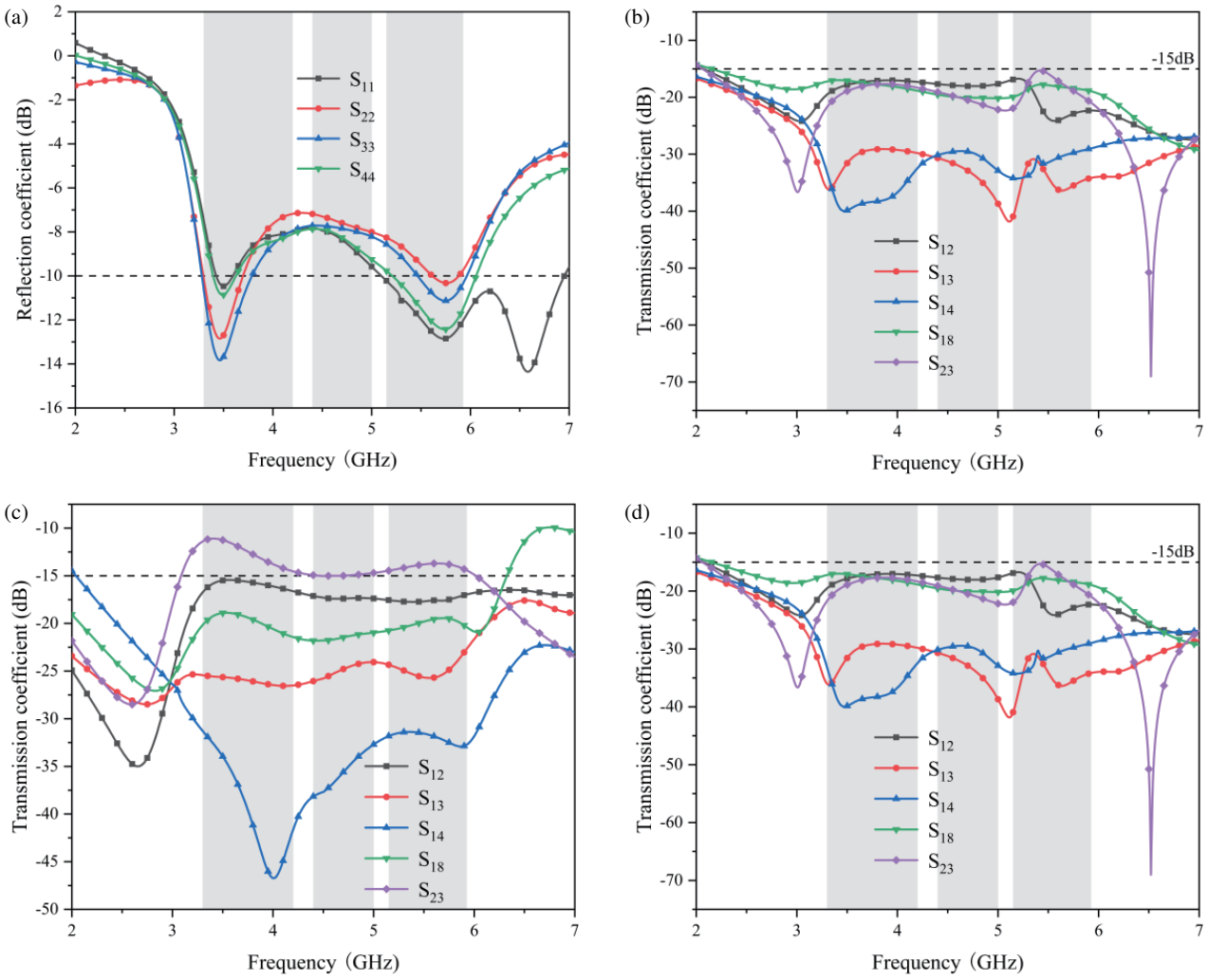

FIGURE 6. Simulated reflection coefficients and transmission coefficients of the proposed antenna array: (a) Reflection coefficients without isolation structure. (b) Reflection coefficients with isolation structure. (c) Transmission coefficients without isolation structure. (d) Transmission coefficients with isolation structure.

coefficients and isolation. Upon comparison, it is evident that the optimized isolated antenna array exhibits superior reflection and transmission coefficients within the desired frequency band.

To gain a deeper understanding of the role played by the isolation structures between antenna elements, the isolation structures are further explored in Fig. 7 and Fig. 8. It is clearly demonstrated that within the required frequency band, the isolation between the antenna elements is significantly enhanced by the presence of isolation structures. The surface current is constrained by the defected ground structure, leading to alterations in its flow length and direction. As a result, the gap between the antenna ports is widened, thereby reducing the coupling between antenna elements.

Moreover, the connection between the mainboard etching and sideboard etching enables high isolation within the 3–6 GHz band. Notably, the L-shaped slot and T-shaped slot prove to effectively enhance the reflection coefficient, as depicted in Fig. 8. By incorporating these slots, each antenna can achieve a wide bandwidth of 3.3–6 GHz, with isolation levels exceeding 15 dB.

Due to the high permittivity and high loss characteristics of the human hand, we have also investigated the impact of user handloading on the performance of the proposed 8-element antenna system. In Fig. 9, the reflection coefficient and transmission coefficient in single-hand mode are provided. It can be observed that, due to the hand's influence on the antenna, antennas 1, 5, and 8 fail to meet the -10 dB impedance bandwidth criterion, resulting in degraded matching levels. However, based on the -6 dB bandwidth criterion, the antennas can still cover the desired frequency band. The isolation level among all antenna elements remains relatively strong, showing improvement compared to the free space scenario and meeting the -15 dB bandwidth criterion, as shown in Fig. 9(b).

In order to show that the mobile phone antenna has application value, it is necessary to explore the influence of hand on the radiation patterns of the antenna. The simulated three-dimensional (3D) radiation patterns are illustrated in Fig. 10

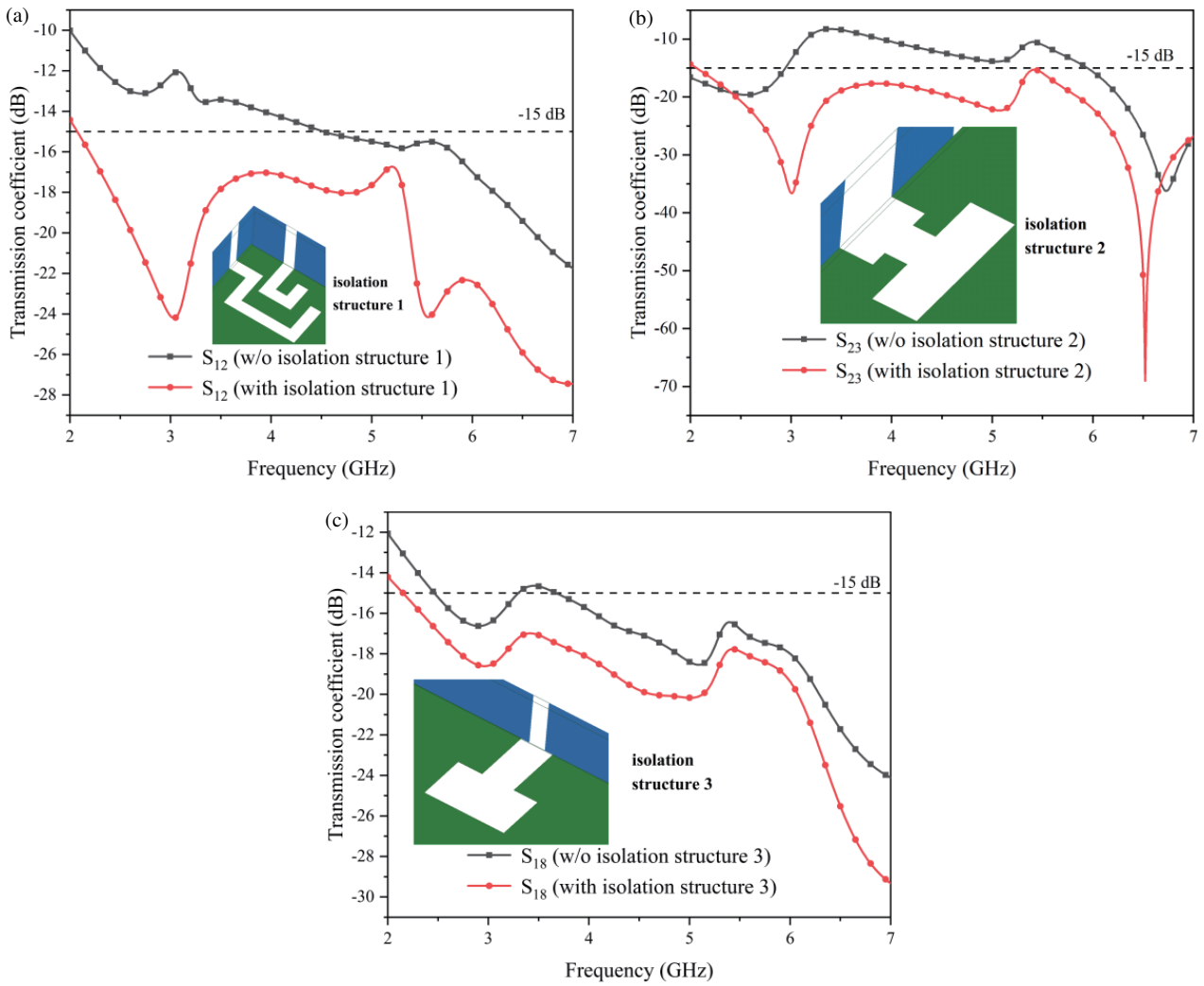

FIGURE 7. Simulated transmission coefficients of the proposed antenna with/without (a) Isolation structure 1. (b) Isolation structure 2. (c) Isolation structure 3.

when Antennas 1 and 2 operate at 3.5 GHz, 4.7 GHz, and 5.5 GHz, respectively. It is obvious from the figure that although Antenna 1 and Antenna 2 have identical geometries, the radiation pattern of each element changes due to different locations on the main board. Taking Antenna 2 as an example, it can be seen that the maximum gain observed in the low resonance mode is 5.2 dBi, while the subsequent maximum gain in the high resonance mode is 8.22 dBi.

Furthermore, Fig. 11 presents the simulation results of the specific absorption rate (SAR) distributions of Antennas 1 and 2 operating independently in three different resonant modes with an input power of 100 mW. SAR serves as a metric for measuring electromagnetic energy absorption in lossy dielectric materials. When being exposed to an external electromagnetic field, the human body generates an induced electromagnetic field. As the human body's various organs act as lossy media, it leads to the generation of current within the body, resulting in the absorption and dissipation of electromagnetic energy. It is evident from Fig. 11 that the maximum SAR of Antennas 1 and 2 is approximately 1 W/kg when they operate at 3.5 GHz, 4.7 GHz, and 5.5 GHz. The results show that the radiation from the mobile phone antenna has little effect on human hands. In addition, it is also possible to observe that the SAR distribution is correlated with the distance of the hand from the antenna element. The closer the distance is, the stronger the radiation effect is, and the SAR distribution is more extensive at low frequencies than the high frequency mode of operation.

4. EXPERIMENTAL RESULTS AND DISCUSSION

For a more comprehensive introduction to the proposed antenna design, we verify the crucial simulation results by measuring the performance of the fabricated prototype antenna, which is illustrated in Fig. 12. The S-parameters of the triple-band mobile MIMO antenna are measured using a PNA N5224A network analyser. In Fig. 13, the simulated and measured reflection coefficients and transmission coefficients are presented. As shown in Fig. 13(a), the simulated and measured bandwidths can cover 3.3–4.2 GHz, 4.4–5 GHz, and 5.15–5.925 GHz. However, due to the manufacturing errors of the

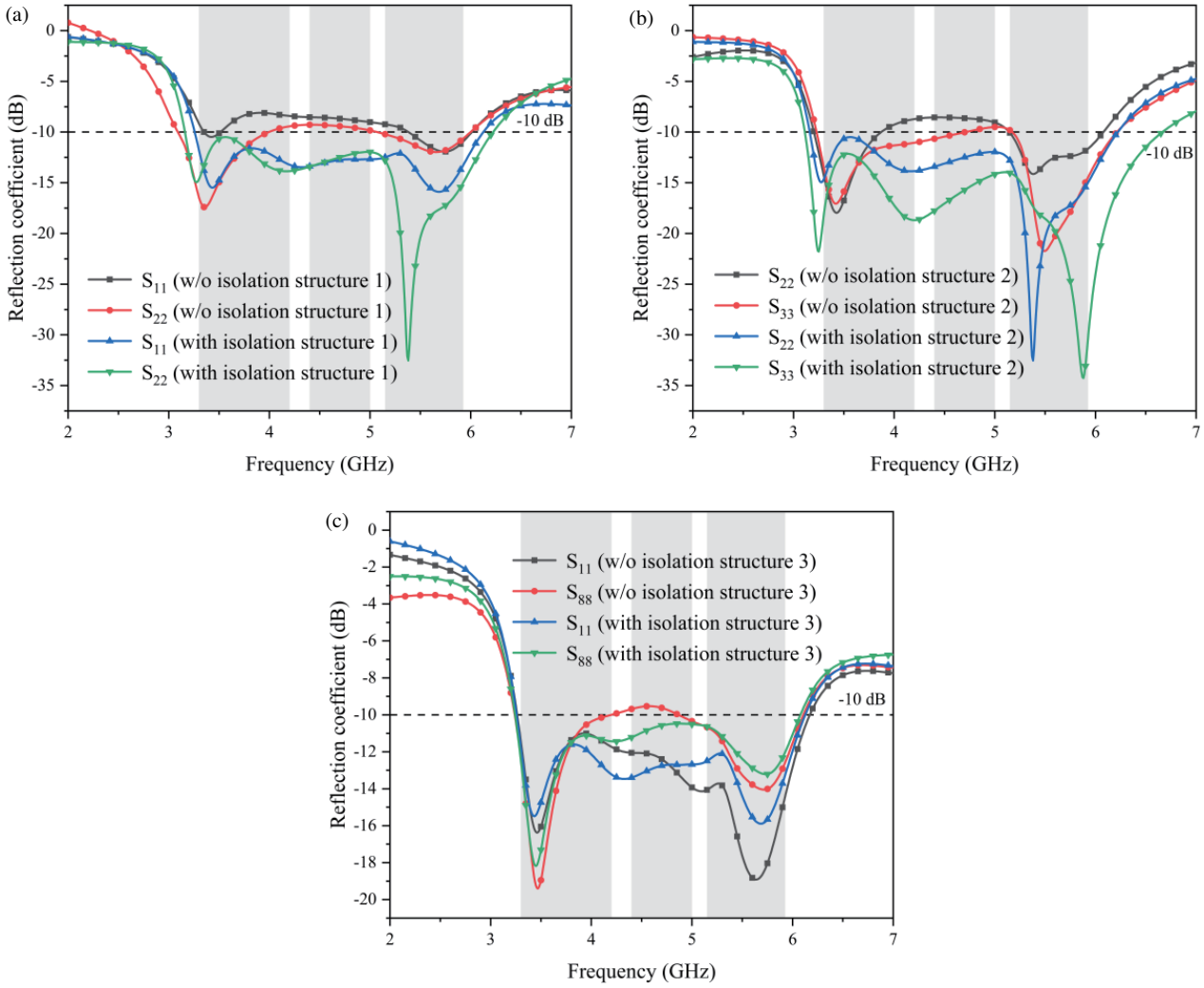

FIGURE 8. Simulated reflection coefficients of the proposed antenna with/without (a) Isolation structure 1. (b) Isolation structure 2. (c) Isolation structure 3.

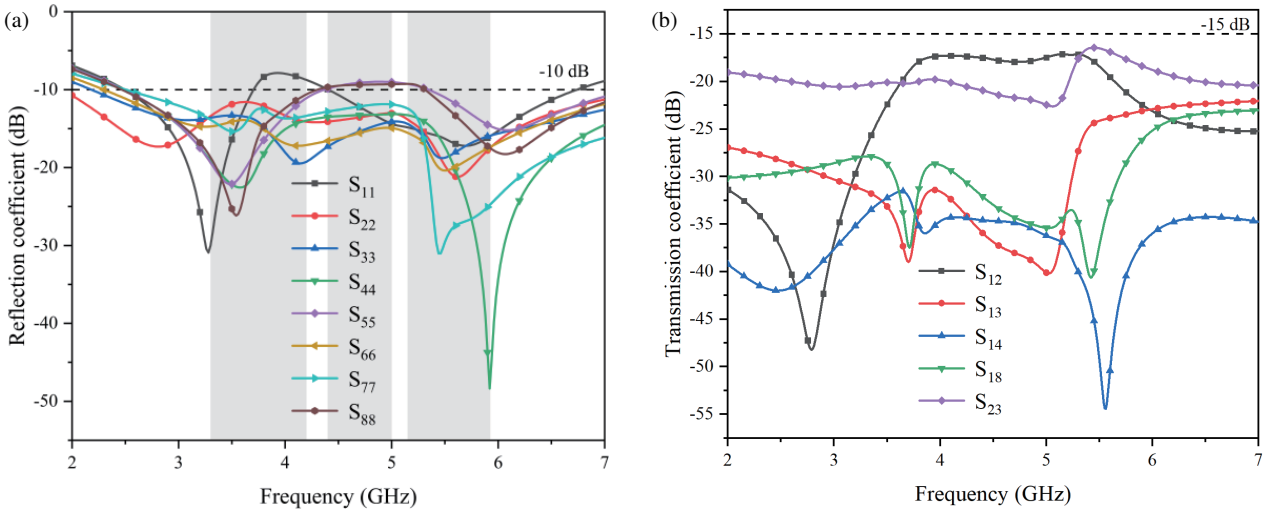

FIGURE 9. Simulated coefficients in single-hand mode (right-hand mode): (a) Reflection coefficient. (b) Transmission coefficient.

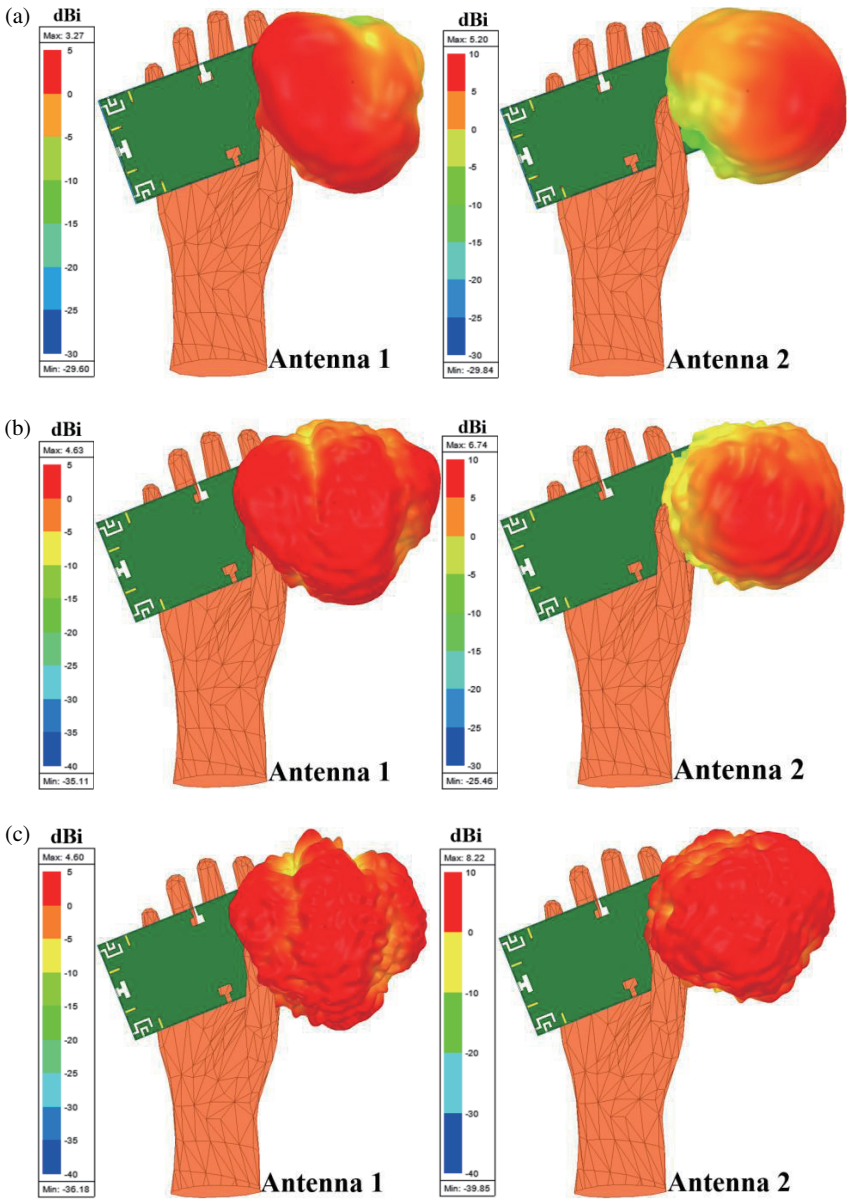

FIGURE 10. Simulated 3D radiation patterns of (a) Ant. 1 and Ant. 2 operating at 3.5 GHz. (b) Ant. 1 and Ant. 2 operating at 4.7 GHz. (c) Ant. 1 and Ant. 2 operating at 5.5 GHz.

SMA connector and the imprecise nature of manual welding, there may be some deviation between the simulation and measurement results. Fig. 13(b) demonstrates that the simulation and measurement results of the optimized antenna prototype can achieve a transmission coefficient of more than −15 dB at 3.3–6 GHz.

As shown in Figs. 14, 15, and 16, the measurement and simulation results of the normalized radiation polarization of the antenna at 3.5 GHz, 4.7 GHz, and 5.5 GHz are given, respectively. The measured cross-polarization and co-polarization are represented by solid black lines and red dashed lines, respectively. It can be observed that all cross-polarization is less than co-polarization, and the same antenna will produce different radiation patterns at various operating frequencies. By comparing the simulated and measured radiation patterns, it can be seen that the simulated far-field radiation pattern is in good agreement with the measured one, and the shape of the radiation pattern is roughly the same. The slight difference may be the error caused by the welding process of the SAM connector. From Fig. 14–Fig. 16, it can also be observed that the antenna element exhibits good radiation performance.

Figure 17 illustrates the total radiation efficiency diagram of the proposed antenna. The results indicate that the total efficiency value ranges from 76% to 88% throughout the entire 3.3–6 GHz band coverage. This demonstrates an acceptable level of efficiency for 5G and WLAN operations. Furthermore, Fig. 18 displays the measured realized peak gain, which is consistently higher than 2.6 dBi and lower than 8 dBi. It can be observed that the curves of radiation efficiency and peak gain exhibit similar trends.

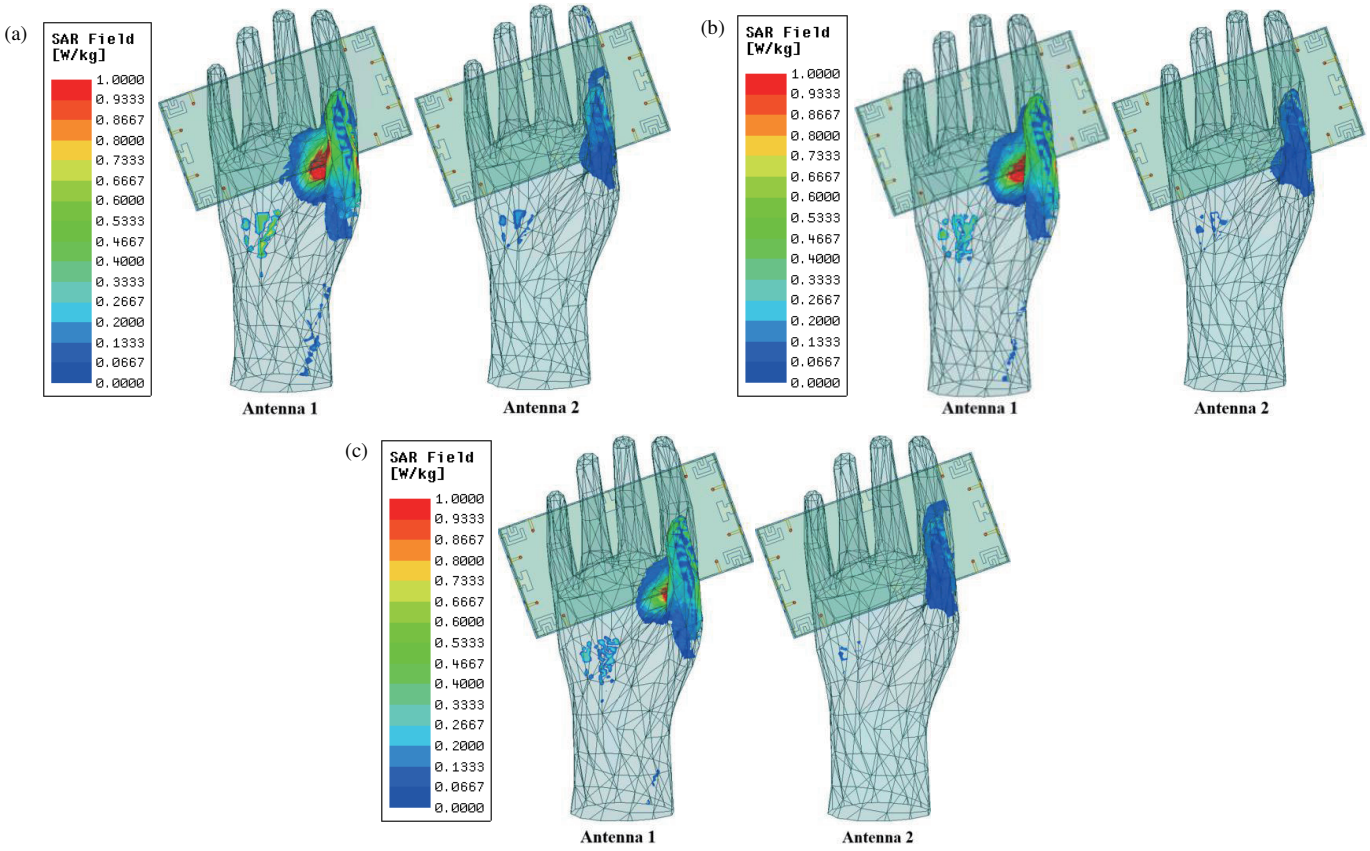

FIGURE 11. Simulation results of SAR field distribution at (a) 3.5 GHz. (b) 4.7 GHz. (c) 5.5 GHz.

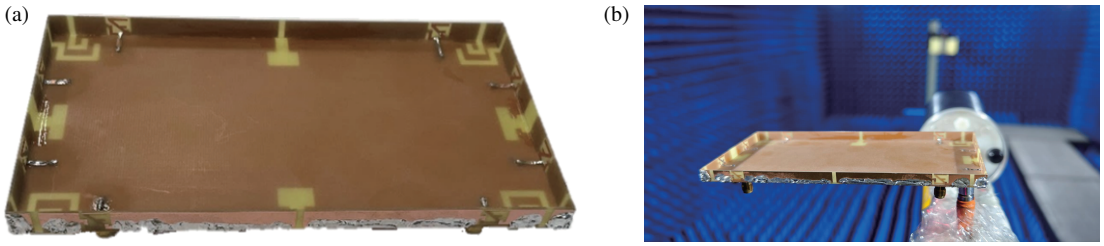

FIGURE 12. Photos of the measurement experiment: (a) Photograph of the antenna prototype. (b) Anechoic chamber.

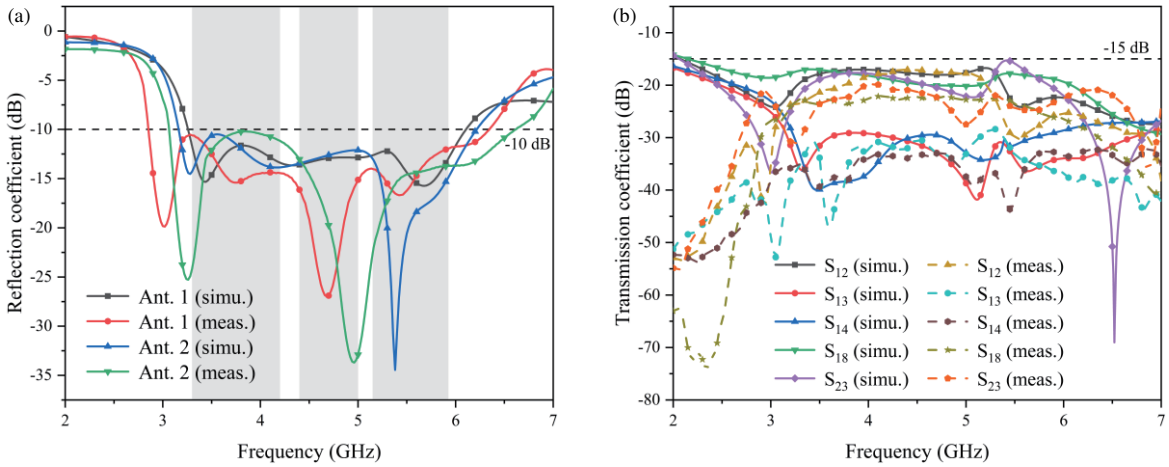

FIGURE 13. Simulation and measurement results of the proposed mobile phone antenna array: (a) Simulated and measured reflection coefficient. (b) Simulated and measured transmission coefficient.

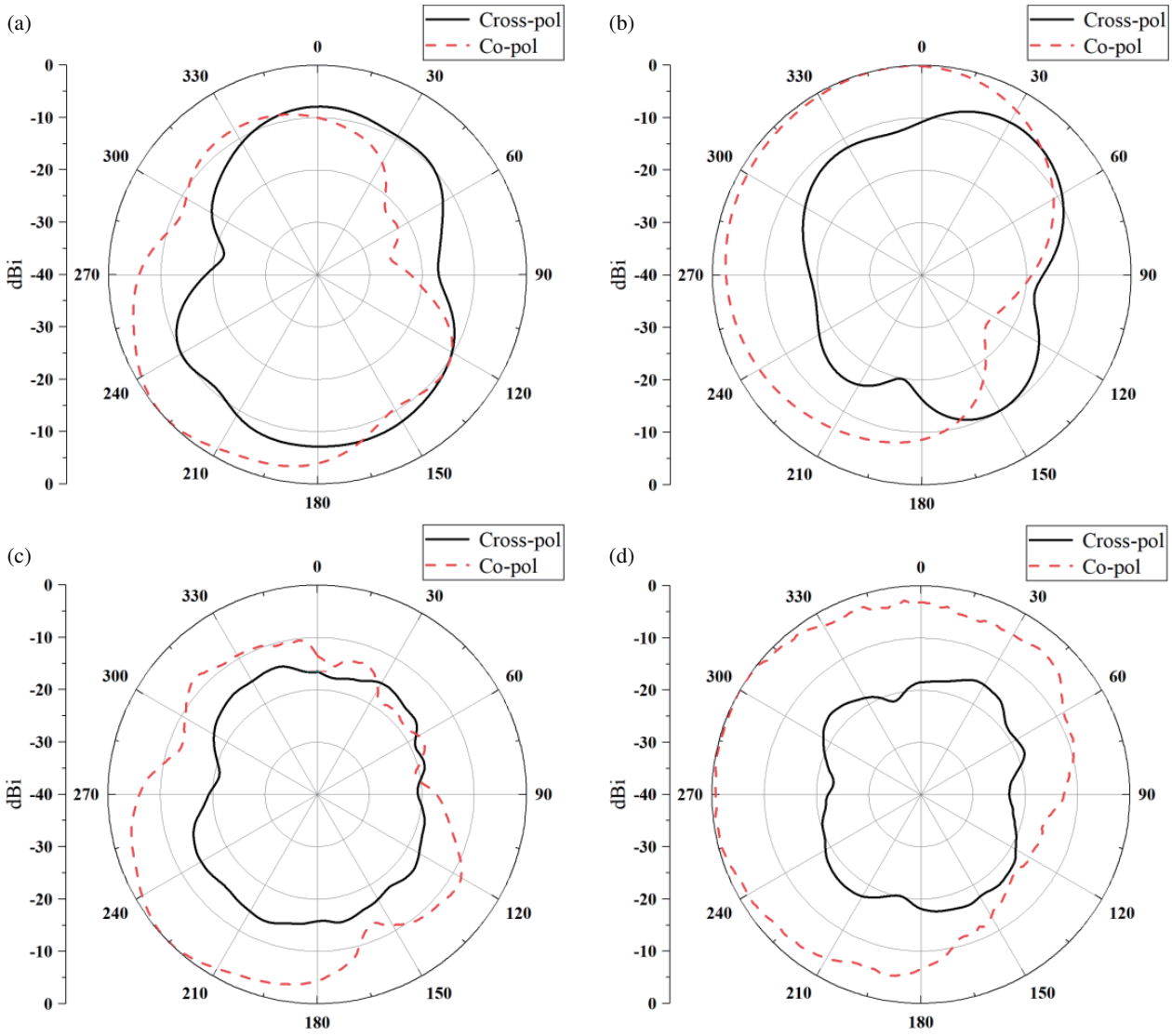

FIGURE 14. Radiation patterns of 3.5 GHz. (a) XOY for simulation. (b) YOZ for simulation. (c) XOY for Measurement. (d) YOZ for Measurement.

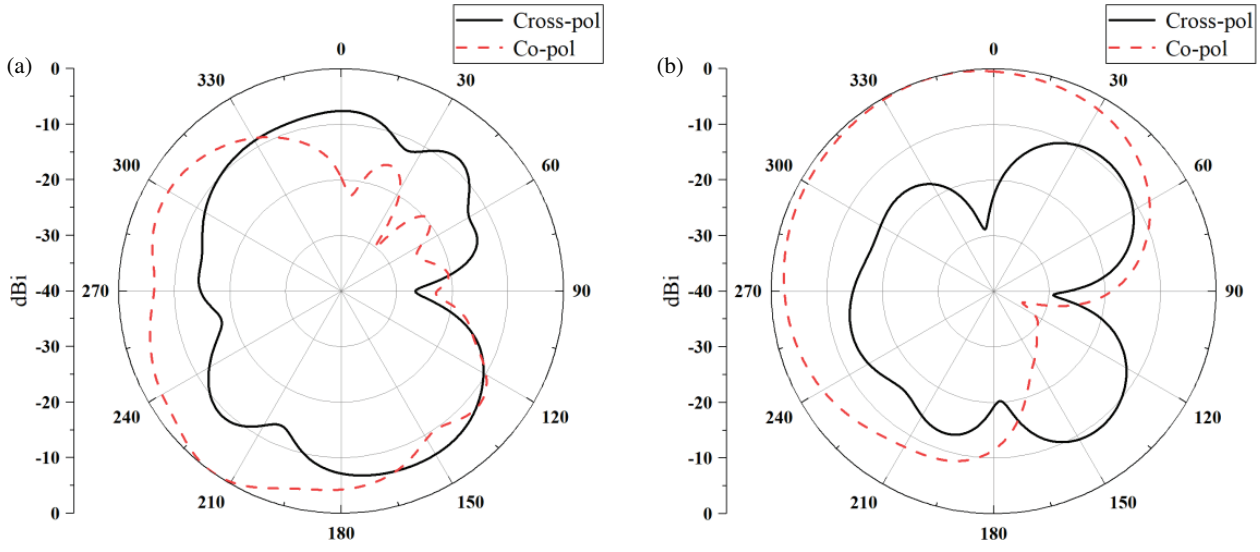

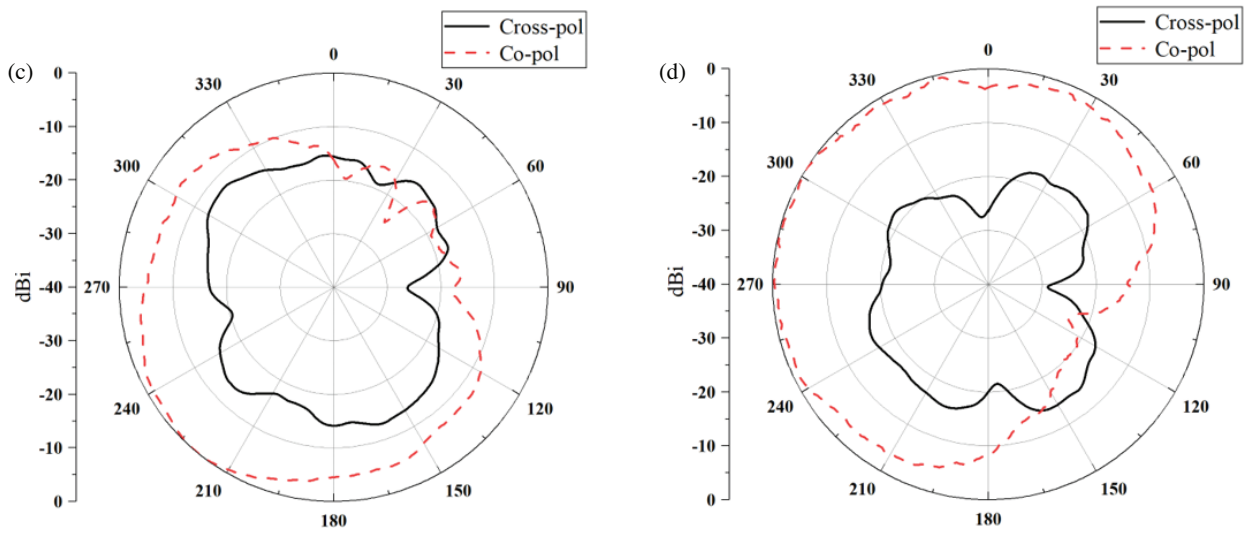

FIGURE 15. Radiation patterns of 4.7 GHz. (a) XOY for simulation. (b) YOZ for simulation. (c) XOY for Measurement. (d) YOZ for Measurement.

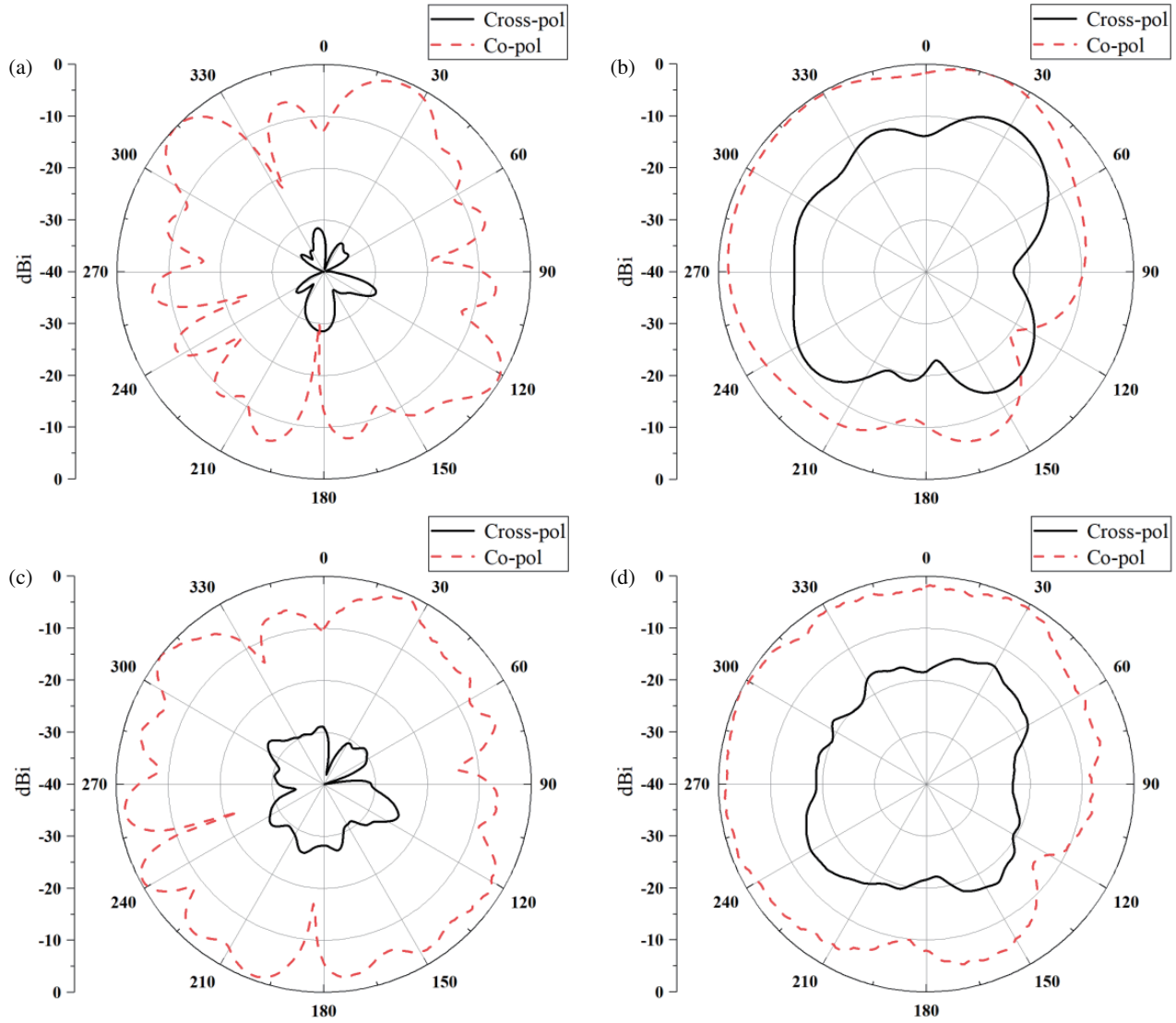

FIGURE 16. Radiation patterns of 5.5 GHz. (a) XOY for simulation. (b) YOZ for simulation. (c) XOY for Measurement. (d) YOZ for Measurement.

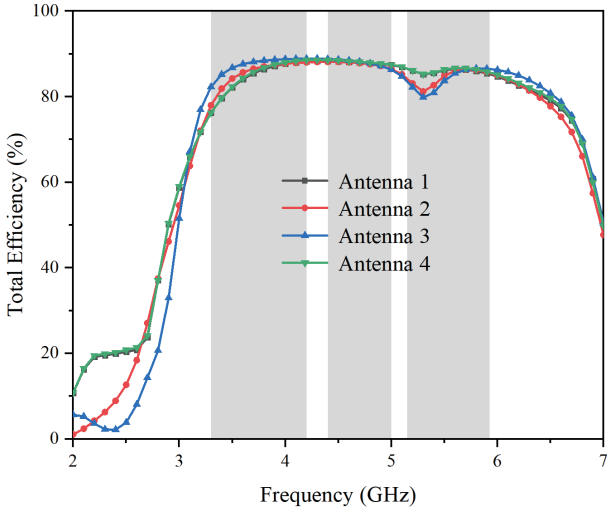

FIGURE 17. Measured total efficiencies of Ant. 1, 2, 3, 4.

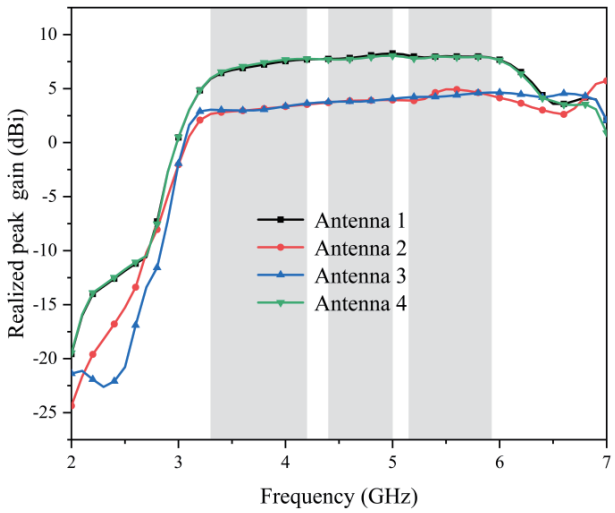

FIGURE 18. Measured realized peak gains of the proposed mobile phone MIMO system.

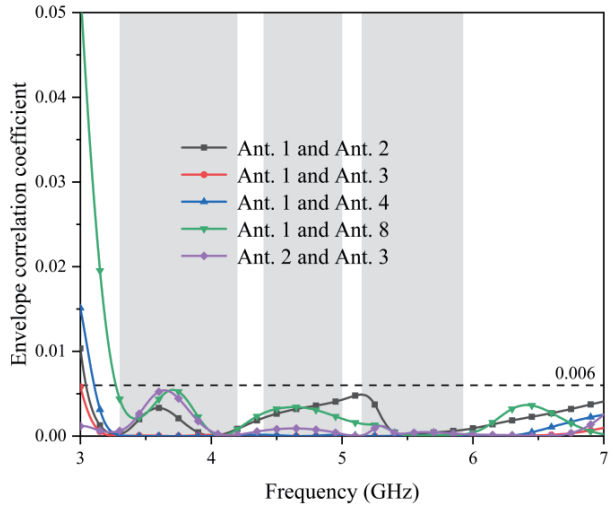

FIGURE 19. The calculated ECC of the proposed triple-band mobile phone antenna array.

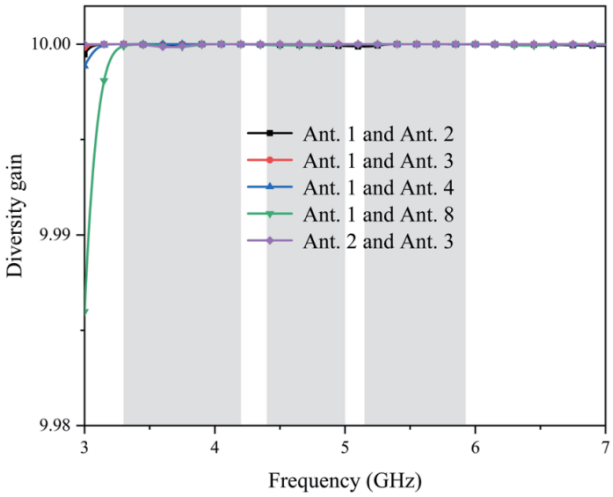

FIGURE 20. Calculated DG of the proposed mobile phone antenna array.

Correlation envelope coefficient (ECC) serves as a parameter to evaluate the diversity and coupling performance of MIMO antenna systems by characterizing the correlation between received signal amplitudes among different antenna elements. High correlation leads to decreased MIMO performance, particularly when envelope correlation exceeds 0.5. This is because MIMO systems rely on the independence of received signals to provide spatial multiplexing diversity and independent channels. ECC can be calculated using the radiation field of the antenna element, as expressed in Eq. (1).

$$\mathrm{ECC} = \frac{\left| \iint_{4\pi} \left[\overrightarrow{F_1}(\theta,\phi) * \overrightarrow{F_2}(\theta,\phi) \right] d\Omega \right|}{\iint_{4\pi} \left| \overrightarrow{F_1}(\theta,\phi) \right|^2 d\Omega \iint_{4\pi} \left| \overrightarrow{F_1}(\theta,\phi) \right|^2 d\Omega} \quad (1)$$

Based on the findings in Fig. 19, it can be inferred that the ECC remains below 0.006 across the entire frequency band of interest, signifying a very low correlation between the antenna elements of the proposed mobile phone MIMO system, which unequivocally meets the acceptable criterion for MIMO operation with an ECC value below 0.5.

The diversity gain (DG) can be calculated using Eq. (2), which is directly influenced by the ECC value.

$$\mathrm{DG} = 10 \times \sqrt{1 - |\mathrm{ECC}|^2} \quad (2)$$

The calculated diversity gain (DG) of the proposed triple-band mobile phone antenna array is depicted in Fig. 20. It is evident that the DG value exceeds 9.99 dB across the frequency band of interest.

In an ideal antenna system where the total antenna efficiency is 100%, and there is no correlation between antennas, multiplexing efficiency (ME) quantifies the power loss in the prototype antenna system concerning the specified capacity. Fig. 21 displays the calculated ME of the proposed triple-band mobile

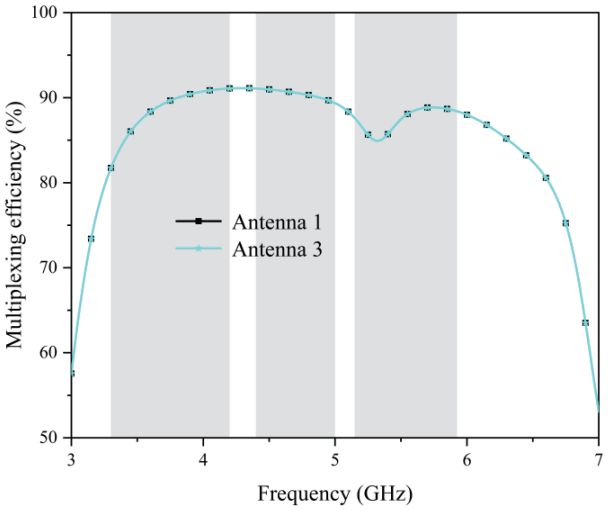

FIGURE 21. Calculated ME of the proposed mobile phone antenna array.

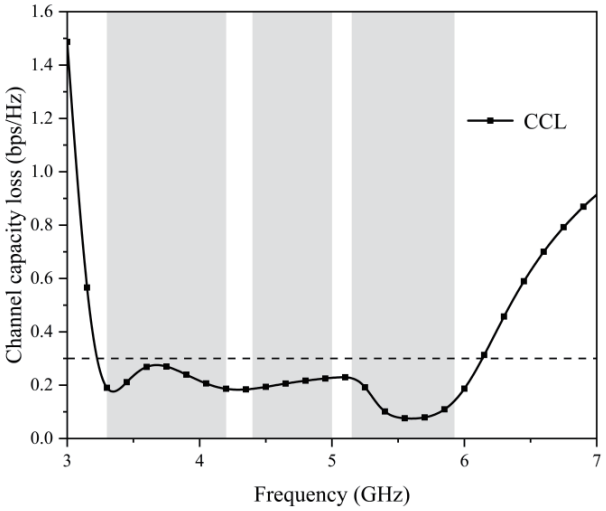

FIGURE 22. Calculated CCL of the proposed mobile phone antenna array.

TABLE 1. Comparison of the proposed design with some referenced works.

Reference	Operating band (GHz)	ECC	CCL (bps/Hz)	DG (dB)	Realized peak gain (dBi)	Total efficiency (%)	Isolation (dB)	Size (mm^3)
[27]	3.3–7.1	< 0.07	< 0.3	/	4.6–6.2	> 48	< -12	$22 \times 22 \times 1.6$
[28]	3.43.8, 4.85, 5.15 5.925	< 0.12	< 0.28	/	2.1–4.8	47–68, 51–67, 43–73	< -10.5	$15 \times 3 \times 1.6$
[29]	3.73.9, 5.65.9	< 0.4	< 0.4	10	2.6–3	78	< -10	$3 \times 30 \times 0.8$
[30]	23, 3.43.9, 4.45.2	< 0.01	< 0.05	10	5.5	/	< -10	$30 \times 40 \times 1.67$
[31]	2.39–2.57, 3.82–6.95	< 0.02	/	> 9.98	2.65	75	< -15	$45 \times 30 \times 1.6$
[32]	3.36.0, 4.8–5.0, 5.15–5.925	< 0.1	< 0.5	> 9.96	/	70–85	< -13	$6.5 \times 7 \times 0.8$
[33]	2–18	< 0.07	/	> 9	2–6.5	70–85	< -20	$48 \times 35 \times 1.6$
[34]	3.2–5.75	< 0.005	< 0.4	> 9.9	9	7891	< -22	$40 \times 40 \times 1.6$
[35]	3.264.48	< 0.068	< 0.4	> 9.95	4.8	60–85	< -14.5	$46 \times 46 \times 1.6$
Proposed	3.3–6.0	< 0.006	< 0.3	> 9.99	2.6–8	76–88	< -15	$7.8 \times 7 \times 0.8$

phone antenna array. The relationship between multiplexing efficiency (ME) and ECC is defined in Eq. (3), where η_1 and η_2 are the total efficiency and their expression Eq. (3):

$$\mathrm{ME} = \sqrt{\eta_1 \eta_2 (1 - |\mathrm{ECC}|^2)} \tag{3}$$

Channel capacity loss (CCL) denotes the decrease in the rate of information transmission in the communication channel without any data loss. The equation for calculating CCL is expressed by Equations (4)–(7)

$$C_{loss} = -\log_2 \left[\det(\psi^R)\right] \tag{4}$$

$$\psi^R = \begin{bmatrix} \rho_{ii} & \rho_{ij} \\ \rho_{ji} & \rho_{jj} \end{bmatrix} \tag{5}$$

$$\rho_{ii} = (1 - |S_{ii}|^2 - |S_{ij}|^2) \tag{6}$$

$$\rho_{ij} = -(S_{ii}{}^* S_{ij} + S_{ji}{}^* S_{ij}) \quad \text{for } i, j = 1 \text{ or } 2 \tag{7}$$

The calculated channel capacity loss (CCL) of the proposed triple-band mobile phone antenna array is illustrated in Fig. 22. It is evident that the CCL value remains below 0.3 across the frequency band of interest. It suggests that the proposed three-band mobile phone antenna demonstrates a highly favorable channel transmission rate.

The proposed design is compared with selected reference works in Table 1, showcasing key parameters such as the operating frequency band, isolation, total efficiency, ECC value, and the size of each measured antenna. The eight-antenna array design exhibits an exceptionally broad operating bandwidth (-10 dB impedance bandwidth) capable of encompassing future 5G NR bands n77/n78/n79 and WLAN. In this study, defected ground structure (DGS) technology is leveraged to enhance bandwidth and isolation, while mutual coupling between different antenna pairs is also addressed. Notably, high isolation levels (> 15 dB) between any two units across the broad-

band spectrum are achieved, surpassing the performance of [29] and [30].

In addition to its wide triple-band operation, the proposed antenna demonstrates outstanding efficiency (76–88%) in comparison to [27] and [28]. Furthermore, the ECC value in this study is notably lower when being juxtaposed with other antennas, underscoring the antenna's superior performance in minimizing correlation between elements.

5. CONCLUSION

This paper presents an investigation into a novel ultra-wideband triple-band 8-element MIMO antenna array designed for 5G smartphone applications. The antenna element is simple in structure and easy to manufacture, and can function effectively within a metal-framed smartphone. The measured -10 dB impedance works in the frequency band from 3.3 GHz to 6 GHz, which can cover 5G bands including N77, N78, N79, and WLAN. By implementing a unique antenna isolation structure between adjacent elements, the coupling between antennas is minimized without compromising basic performance. The proposed triple-band 8-element MIMO antenna exhibits low mutual couplings of less than -15 dB. Due to these features, it is an attractive option for future 5G MIMO mobile communication systems. Additionally, the antenna showcases high efficiency ($> 76\%$), low ECC (< 0.006), and minimal channel capacity loss, which collectively improve the antenna's overall performance. These results demonstrate the potential of the proposed design and its ability to address the demands of next-generation wireless communication systems.

ACKNOWLEDGEMENT

This work was supported in part by the National Natural Science Foundation of China under Grant No. 6167133, the Science and Technology Department of Zhejiang Province under Grant No. LGG19F010009, and Wenzhou Municipal Science and Technology Program under Grant No. 2018ZG019.

REFERENCES

[1] Sun, L., Y. Li, Z. Zhang, and Z. Feng, "Wideband 5G MIMO antenna with integrated orthogonal-mode dual-antenna pairs for metal-rimmed smartphones," *IEEE Transactions on Antennas and Propagation*, Vol. 68, No. 4, 2494–2503, 2020.

[2] Garikipati, S., G. Tangirala, M. K. C. Durbhakula, and V. K. Sharma, "Reconfigurable grounds MIMO antenna with PIN diodes for 5G NR n3/n1/n40/n41/n77/n79 to X-bands," *International Journal of Electronics*, Vol. 111, No. 8, 1361–1383, 2024.

[3] Parchin, N. O., Y. I. A. Al-Yasir, J. M. Noras, and R. A. Abd-Alhameed, "Dual-polarized MIMO antenna array design using miniaturized self-complementary structures for 5G smartphone applications," in *2019 13th European Conference on Antennas and Propagation (EuCAP)*, 1–4, Krakow, Poland, Mar. 2019.

[4] Li, Y., Y. Luo, G. Yang, *et al.*, "High-isolation 3.5 GHz eight-antenna MIMO array using balanced open-slot antenna element for 5G smartphones," *IEEE Transactions on Antennas and Propagation*, Vol. 67, No. 6, 3820–3830, 2019.

[5] Cui, L., J. Guo, Y. Liu, *et al.*, "An 8-element dual-band MIMO antenna with decoupling stub for 5G smartphone applications," *IEEE Antennas and Wireless Propagation Letters*, Vol. 18, No. 10, 2095–2099, 2019.

[6] Cheng, B. and Z. Du, "Dual polarization MIMO antenna for 5G mobile phone applications," *IEEE Transactions on Antennas and Propagation*, Vol. 69, No. 7, 4160–4165, 2021.

[7] Khan, R., A. A. Al-Hadi, P. J. Soh, M. R. Kamarudin, M. T. Ali, *et al.*, "User influence on mobile terminal antennas: A review of challenges and potential solution for 5G antennas," *IEEE Access*, Vol. 6, 77 695–77 715, 2018.

[8] Xu, H., H. Wang, S. Gao, H. Zhou, Y. Huang, Q. Xu, and Y. Cheng, "A compact and low-profile loop antenna with six resonant modes for LTE smartphone," *IEEE Transactions on Antennas and Propagation*, Vol. 64, No. 9, 3743–3751, 2016.

[9] Hu, W., L. Qian, S. Gao, L.-H. Wen, Q. Luo, H. Xu, X. Liu, Y. Liu, and W. Wang, "Dual-band eight-element MIMO array using multi-slot decoupling technique for 5G terminals," *IEEE Access*, Vol. 7, 153 910–153 920, 2019.

[10] Chang, L., Y. Yu, K. Wei, and H. Wang, "Polarization-orthogonal co-frequency dual antenna pair suitable for 5G MIMO smartphone with metallic bezels," *IEEE Transactions on Antennas and Propagation*, Vol. 67, No. 8, 5212–5220, 2019.

[11] Chang, L., Y. Yu, K. Wei, and H. Wang, "Orthogonally polarized dual antenna pair with high isolation and balanced high performance for 5G MIMO smartphone," *IEEE Transactions on Antennas and Propagation*, Vol. 68, No. 5, 3487–3495, 2020.

[12] Patel, U. and T. Upadhyaya, "Four-port dual-band multiple-input multiple-output dielectric resonator antenna for sub-6 GHz 5G communication applications," *Micromachines*, Vol. 13, No. 11, 2022, 2022.

[13] Agiwal, M., A. Roy, and N. Saxena, "Next generation 5G wireless networks: A comprehensive survey," *IEEE Communications Surveys & Tutorials*, Vol. 18, No. 3, 1617–1655, 2016.

[14] Li, M.-Y., Y.-L. Ban, Z.-Q. Xu, J. Guo, and Z.-F. Yu, "Tri-polarized 12-antenna MIMO array for future 5G smartphone applications," *IEEE Access*, Vol. 6, 6160–6170, 2017.

[15] Wong, K.-L., C.-Y. Tsai, and J.-Y. Lu, "Two asymmetrically mirrored gap-coupled loop antennas as a compact building block for eight-antenna MIMO array in the future smartphone," *IEEE Transactions on Antennas and Propagation*, Vol. 65, No. 4, 1765–1778, 2017.

[16] Dong, J., S. Wang, and J. Mo, "Design of a twelve-port MIMO antenna system for multi-mode 4G/5G smartphone applications based on characteristic mode analysis," *IEEE Access*, Vol. 8, 90 751–90 759, 2020.

[17] Sghaier, N. and L. Latrach, "Design and analysis of wideband MIMO antenna arrays for 5G smartphone application," *International Journal of Microwave and Wireless Technologies*, Vol. 14, No. 4, 511–523, 2022.

[18] Wang, S. and Z. Du, "Decoupled dual-antenna system using crossed neutralization lines for LTE/WWAN smartphone applications," *IEEE Antennas and Wireless Propagation Letters*, Vol. 14, 523–526, 2014.

[19] Guo, J., L. Cui, C. Li, and B. Sun, "Side-edge frame printed eight-port dual-band antenna array for 5G smartphone applications," *IEEE Transactions on Antennas and Propagation*, Vol. 66, No. 12, 7412–7417, 2018.

[20] Ghalib, A. and M. S. Sharawi, "TCM analysis of defected ground structures for MIMO antenna designs in mobile terminals," *IEEE Access*, Vol. 5, 19 680–19 692, 2017.

[21] Sim, C.-Y.-D., H.-Y. Liu, and C.-J. Huang, "Wideband MIMO antenna array design for future mobile devices operating in the 5G NR frequency bands n77/n78/n79 and LTE band 46," *IEEE Antennas and Wireless Propagation Letters*, Vol. 19, No. 1, 74–

78, 2020.

[22] Zhou, C. F., J. X. Sun, and H. Li, "Wideband MIMO antenna with decoupling slots for 5G smartphone applications," in *2021 International Symposium on Antennas and Propagation (ISAP)*, 1–3, Taipei, Taiwan, Oct. 2021.

[23] Li, M.-Y., Y.-L. Ban, Z.-Q. Xu, G. Wu, K. Kang, *et al.*, "Eight-port orthogonally dual-polarized antenna array for 5G smartphone applications," *IEEE Transactions on Antennas and Propagation*, Vol. 64, No. 9, 3820–3830, 2016.

[24] Zhao, X., S. P. Yeo, and L. C. Ong, "Decoupling of inverted-F antennas with high-order modes of ground plane for 5G mobile MIMO platform," *IEEE Transactions on Antennas and Propagation*, Vol. 66, No. 9, 4485–4495, 2018.

[25] Li, Y., Y. Luo, G. Yang, *et al.*, "Multiband 10-antenna array for sub-6 GHz MIMO applications in 5-G smartphones," *IEEE Access*, Vol. 6, 28 041–28 053, 2018.

[26] Hei, Y. Q., J. G. He, and W. T. Li, "Wideband decoupled 8-element MIMO antenna for 5G mobile terminal applications," *IEEE Antennas and Wireless Propagation Letters*, Vol. 20, No. 8, 1448–1452, 2021.

[27] Sghaier, N. and L. Latrach, "Design and analysis of wideband MIMO antenna arrays for 5G smartphone application," *International Journal of Microwave and Wireless Technologies*, Vol. 14, No. 4, 511–523, 2021.

[28] Wang, H., R. Zhang, Y. Luo, and G. Yang, "Compact eight-element antenna array for triple-band MIMO operation in 5G mobile terminals," *IEEE Access*, Vol. 8, 19 433–19 449, 2020.

[29] Jha, P., A. Kumar, D. Sahu, and N. Sharma, "Isolation enhancement of two element MIMO antenna based on neutralization technique," in *2023 3rd International Conference on Advancement in Electronics & Communication Engineering (AECE)*, 355–359, Ghaziabad, India, 2023.

[30] Ghadeer, S. H., S. K. A. Rahim, M. Alibakhshikenari, B. S. Virdee, T. A. Elwi, A. Iqbal, and M. Al-Hasan, "An innovative fractal monopole MIMO antenna for modern 5G applications," *AEU — International Journal of Electronics and Communications*, Vol. 159, 154480, 2023.

[31] Dhasarathan, V., T. K. Tran, J. Kulkarni, B. A. Garner, Y. Li, *et al.*, "Mutual coupling reduction in dual-band MIMO antenna using parasitic dollar-shaped structure for modern wireless communication," *IEEE Access*, Vol. 11, 5617–5628, 2023.

[32] Huang, J., Z. Chen, Q. Cai, T. H. Loh, and G. Liu, "Minimized triple-band eight-element antenna array for 5G metal-frame smartphone applications," *Micromachines*, Vol. 13, No. 1, 136, 2022.

[33] Sakli, H., C. Abdelhamid, C. Essid, and N. Sakli, "Metamaterial-based antenna performance enhancement for MIMO system applications," *IEEE Access*, Vol. 9, 38 546–38 556, 2021.

[34] Megahed, A. A., M. Abdelazim, E. H. Abdelhay, and H. Y. M. Soliman, "Sub-6 GHz highly isolated wideband MIMO antenna arrays," *IEEE Access*, Vol. 10, 19 875–19 889, 2022.

[35] Kiani, S. H., M. E. Munir, H. S. Savci, H. Rimli, E. Alabdulkreem, H. Elmannai, G. Pau, and M. Alibakhshikenari, "Dual-polarized wideband 5G N77 band slotted MIMO antenna system for next-generation smartphones," *IEEE Access*, Vol. 12, 34 467–34 476, 2024.